Instabilities for absorptive optical bistability in a nonideal Fabry-Pérot cavity

A. J. van Wonderen and L. G. Suttorp
Institute for Theoretical Physics, Valckenierstraat 65, 1018 XE Amsterdam, The Netherlands
(Received 5 April 1989)

Instabilities are predicted for absorptive optical bistability in a nonideal Fabry-Pérot cavity on the basis of Maxwell-Bloch theory. We show that the stability problem of the Maxwell-Bloch equations can be formulated in terms of a Riccati differential equation with boundary conditions. We have integrated this equation numerically. Our results crucially depend on the value of the transmission coefficient of the mirrors. For finite values of this quantity we find that the nearest side mode is responsible for two disconnected instability domains in the plane spanned by the output intensity and the medium response time. One of these domains can generate instabilities in the upper and the lower branch of the steady-state curve if the cooperation parameter is sufficiently large. Higher side modes can give rise to positive-slope instabilities as well. From our findings it can be understood why a recent experimental search for instabilities in absorptive optical bistability has led to a negative result. We finally demonstrate that the instability spectra of a Fabry-Pérot cavity and a so-called equivalent ring cavity differ considerably.

I. INTRODUCTION

The study of instabilities in optical bistability is of fundamental importance because it gives insight in the behavior of systems driven far from thermodynamic equilibrium. Recognition of this fact has been a motive for numerous investigations which have deepened our understanding of time-dependent phenomena in passive media.[1] In most of these treatments an external feedback of the laser beam has been chosen by adopting a ring geometry; with this choice standing-wave complications are avoided. For systems with internal feedback, such as the Fabry-Pérot arrangement, instabilities have only been examined with the help of simplified semiclassical theories. For example, equations with a third-order nonlinearity[2-4] and delay-differential equations[5-8] have been used. The treatments that employ the full Maxwell-Bloch formalism generally adopt the uniform-field approximation.[9-12] This approximation is only reliable if the cavity is equipped with almost ideal mirrors. It remains to be seen whether uniform-field predictions on instabilities also hold for a nonideal Fabry-Pérot cavity, as used in recent experiments.[13-15]

In this paper we intend to analyze the instability spectrum of an optically bistable nonlinear medium contained in a Fabry-Pérot cavity with mirrors of finite transmission coefficient. As a basis we shall use the analytical results that we have derived in an earlier paper.[16] In this way we are able to predict the complete multimode instability spectrum; it will not be necessary to invoke a single-mode approximation.[17] The medium is assumed to consist of homogeneously broadened two-level particles described by the Maxwell-Bloch equations. As in previous work[9-12] both the particles and the cavity are assumed to be in perfect resonance with the incident laser beam. Furthermore, we shall use the plane-wave approximation so that transverse effects are not taken into account.[18]

The stability of a stationary state of an optically bistable system can be investigated by evaluating the effect of a small time-dependent perturbation on the transmitted light beam. In the plane-wave approximation this light beam is described by the electric field $E_T^{(\mathrm{st})}\exp[i(kz-\omega t)]+\mathrm{c.c.}$, with ω the frequency of the laser and $k=\omega/c$. The amplitude $E_T^{(\mathrm{st})}$ can be chosen to be real and positive; its superscript (st) indicates that the incident laser beam is kept stationary. If we add a small perturbation $\delta E_T(t)$ to the transmitted amplitude $E_T^{(\mathrm{st})}$, the output electric field becomes

$$[E_T^{(\mathrm{st})}+\delta|E_T(t)|]\exp(i\{kz-\omega t+\delta\arg[E_T(t)]\})+\mathrm{c.c.} \tag{1.1}$$

Both the amplitude deviation $\delta|E_T(t)|$ and the phase deviation $\delta\arg[E_T(t)]$ can be determined from the linearized Maxwell-Bloch equations. For the former deviation we find

$$\delta|E_T(t)|=\sum_l c_l\Delta E_{T,l}\exp(\lambda_l t)\ . \tag{1.2}$$

The complex eigenvalues λ_l are the solutions of a stability problem that we have discussed lately.[16] Since the eigenvalues occur in pairs of complex conjugates, the right-hand side of (1.2) can be chosen to be real.

Obviously the stability of the output beam depends on the sign of $\mathrm{Re}\lambda_l$. If $\mathrm{Re}\lambda_l$ is positive for a given l the amplitude of the transmitted electric field deviates from the stationary amplitude after a time of the order of $|\mathrm{Re}\lambda_l|^{-1}$. A contribution of the form

$$\tilde{E}_T\exp[ikz-i(\omega-\mathrm{Im}\lambda_l)t] \tag{1.3}$$

develops, with $|\tilde{E}_T|$ comparable to E_T. If $\mathrm{Im}\lambda_l$ equals zero this contribution is generated by the cavity mode which is in resonance with the laser frequency ω. In the case that $\mathrm{Im}\lambda_l$ is of the order of the free spectral range

$\pi c/L$, the cavity mode nearest to the resonant mode is responsible for the instability. The output signal can then display beats with frequency $\mathrm{Im}\lambda_I$, as a consequence of the interference of the side-mode contribution with the resonant light wave.

In Sec. II we derive a differential equation with boundary conditions from which the eigenvalue λ that governs amplitude instabilities can be computed numerically.[19] Predictions on instabilities are then made in Sec. III. Particular attention is paid to the question whether a part of the steady-state curve with a positive slope can become unstable. Finally, we compare our predictions with experimental findings that have been reported lately.[13–15]

II. FORMULATION OF THE AMPLITUDE STABILITY PROBLEM

A linear stability analysis of the Maxwell-Bloch equations for the case of a Fabry-Pérot cavity leads to the following set of differential equations[1,16]

$$\frac{d\Delta f}{d\zeta}=-\frac{\lambda L}{c}\Delta f+CT\Delta P_{F,1}\ , \tag{2.1}$$

$$-\frac{d\Delta b}{d\zeta}=-\frac{\lambda L}{c}\Delta b+CT\Delta P_{B,1}\ , \tag{2.2}$$

where Δf and Δb denote deviations of the amplitudes of the forward and the backward electric field. These deviations depend on the scaled spatial variable $\zeta=z/L$, with L the length of the cavity. The right-hand sides of (2.1) and (2.2) consist of a term proportional to the eigenvalue λ of the stability problem and a contribution originating from the presence of a nonlinear medium. The influence of the medium is determined by the product of the cooperation parameter $C=\alpha L/T$, with α the medium absorption coefficient, and the transmission coefficient of the mirrors $T=1-R$.

The quantities $\Delta P_{F,1}$ and $\Delta P_{B,1}$ are the amplitude deviations of the slowly varying first harmonic of the forward and the backward polarization fields, respectively. They can be obtained in terms of the deviations Δf and Δb by solving the linearized Bloch equations for amplitude deviations. These algebraic equations can be written down formally as

$$\underline{A}(\zeta)\cdot\Delta\mathbf{x}(\zeta)=\mathbf{F}(\zeta)\Delta f+\mathbf{B}(\zeta)\Delta b\ . \tag{2.3}$$

The infinite-dimensional vector $\Delta\mathbf{x}$ is made up of the amplitude deviations of all polarization envelopes $\{P_{F,m},P_{B,m}\}_{m=1}^{\infty}$ and all inversion envelopes $\{D_m\}_{m=0}^{\infty}$. The matrix $\underline{A}$ and the vectors $\mathbf{F}$ and $\mathbf{B}$ depend on the stationary fields and the eigenvalue λ. It may be noted here that for the case of unidirectional propagation the dimensionality of the set (2.3) reduces to 2.

In order to find the deviations $\Delta P_{F,1}$ and $\Delta P_{B,1}$ from (2.3) we perform as a first step a truncation of the harmonic expansion for the polarization and the inversion

$$P_{F,m}(\zeta,t)=P_{B,m}(\zeta,t)=D_m(\zeta,t)=0\ , \tag{2.4}$$

for $m>N$, N a positive integer. On eliminating subsequently all polarization envelopes the system (2.3) becomes a $(N+1)$-dimensional matrix equation for the deviations $\{\Delta D_m\}_{m=0}^{N}$. Owing to the band structure of the matrix the elements of its inverse can be found directly in terms of Chebyshev polynomials; the argument of these polynomials is a certain combination of the stationary forward and backward electric fields f and b, the medium damping coefficients $\gamma_\perp$ and $\gamma_\parallel$, and the eigenvalue λ.[16] Once the appropriate elements of the inverse matrix have been computed one can derive the desired expressions for $\Delta P_{F,1}$ and $\Delta P_{B,1}$. However, these expressions still depend on the truncation parameter N: in order to take the standing-wave effects fully into account they must be considered in the limiting case $N\to\infty$. This can be done in a systematic way by employing the properties and the representations of Chebyshev polynomials.[20]

We remark that the program described above can be applied to the dispersive case as well. We shall demonstrate this in a future publication. For the purely absorptive case, which is studied in this paper, one ends up with the following two-dimensional set of linear differential equations:

$$\frac{d}{d\zeta}\begin{bmatrix}\Delta f\\ \Delta b\end{bmatrix}=\begin{bmatrix}H_{11} & H_{12}\\ H_{21} & H_{22}\end{bmatrix}\begin{bmatrix}\Delta f\\ \Delta b\end{bmatrix}\ . \tag{2.5}$$

The matrix elements H_{ij} are given by the following expressions:[16]

$$H_{11}=-\frac{\lambda L}{c}+CT\frac{1+\lambda_\perp^{-1}}{16f^2}\left[1+\frac{(1-4f^2+4b^2)^2}{4(\lambda_p-1)W}+\frac{(1-4f_\lambda^2+4b_\lambda^2)^2}{4(\lambda_p^{-1}-1)W_\lambda}\right]-CT\frac{\lambda_\perp^{-1}}{4W}\ , \tag{2.6}$$

$$H_{12}=CT\frac{1+\lambda_\perp^{-1}}{16fb}\left[1+\frac{1-(4f^2-4b^2)^2}{4(\lambda_p-1)W}+\frac{1-(4f_\lambda^2-4b_\lambda^2)^2}{4(\lambda_p^{-1}-1)W_\lambda}\right]+CT\lambda_\perp^{-1}\frac{1+4f^2+4b^2-4W}{32fbW}\ , \tag{2.7}$$

and by the symmetry relations

$$H_{21}(f,b)=-H_{12}(b,f)\ ,\qquad H_{22}(f,b)=-H_{11}(b,f)\ . \tag{2.8}$$

Here the quantity λ_p stands for the product $\lambda_\perp\lambda_\parallel$, with $\lambda_i=1+\gamma_i^{-1}\lambda$ for $i=\perp,\parallel$. Furthermore we have introduced the scaled amplitudes $f_\lambda=\lambda_p^{-1/2}f$ and $b_\lambda=\lambda_p^{-1/2}b$. The symbol W is defined as

$$4W=[1+8(f^2+b^2)+16(f^2-b^2)^2]^{1/2}\ . \tag{2.9}$$

Likewise W_λ is given by a square-root containing f_λ and b_λ instead of f and b. Hence W_λ is complex; the

prescription

$$\mathrm{Re}\left[\frac{W_\lambda}{1+4f_\lambda^2+4b_\lambda^2}\right]>0 \tag{2.10}$$

determines its sign.

Both f and b depend on ζ in a way determined by the stationary Maxwell-Bloch equations.[21] To be specific, they are given by the relation[16]

$$\{f^2-b^2+[(f^2-b^2)^2+\tfrac{1}{8}-\tfrac{1}{2}K]^{1/2}\}\exp(4f^2-4b^2) =(K-\tfrac{1}{4}+\tfrac{1}{2}x^2)\exp[2CT(1-\zeta)+Tx^2] \tag{2.11}$$

and the constraint

$$f^2+b^2=\tfrac{1}{4}-K+[(f^2-b^2)^2+\tfrac{1}{8}-\tfrac{1}{2}K]^{1/2}, \tag{2.12}$$

where K is defined as

$$4K=-x^2(1+R)+[T^2x^4+2x^2(1+R)+1]^{1/2}, \tag{2.13}$$

with x the amplitude of the stationary transmitted field.

The Fabry-Pérot arrangement imposes two boundary conditions on the set of differential equations (2.5). These conditions read

$$\Delta f(0)=R^{1/2}\Delta b(0),\quad \Delta f(1)=R^{-1/2}\Delta b(1). \tag{2.14}$$

They can only be met for a particular value of the eigenvalue λ, which is thus determined as a function of x, C, T, $\gamma_\perp$, and $\gamma_\parallel$.

Although the system (2.5) is linear, it cannot be solved easily: the spatial dependence of the matrix $\underline{H}$ presents us with an ordering problem. We avoid this difficulty by defining $Q=\Delta f/\Delta b$. From (2.5) we infer that Q satisfies the differential equation

$$\frac{dQ}{d\zeta}=H_{12}(Q^2+1)+(H_{11}-H_{22})Q. \tag{2.15}$$

This nonlinear equation is of the Riccati type.[22] It has to be solved with the boundary conditions

$$Q(0)=R^{1/2},\quad Q(1)=R^{-1/2}. \tag{2.16}$$

The coefficients of the Riccati equation (2.15) depend on the stationary fields f and b, which themselves are functions of ζ. In order to write the Riccati equation in a closed form we exploit our knowledge of the spatial dependence of the stationary fields. Instead of ζ we introduce as a new independent variable

$$\chi=2f^2+2b^2+2K-\tfrac{1}{2}, \tag{2.17}$$

with the constant K as given by (2.13). From (2.9) and (2.12) we directly obtain the identities needed to write the right-hand side of (2.15) in terms of χ

$$f^2-b^2=\tfrac{1}{2}(\chi^2-A^2)^{1/2}, \tag{2.18}$$

$$4fb=A(2\chi+A^2+1)^{1/2}, \tag{2.19}$$

$$W=\tfrac{1}{2}(\chi+\tfrac{1}{2}), \tag{2.20}$$

$$W_\lambda=\tfrac{1}{4}[(2\lambda_p^{-1}\chi+1)^2+4\lambda_p^{-1}A^2(1-\lambda_p^{-1})]^{1/2}, \tag{2.21}$$

with $A=(\frac{1}{2}-2K)^{1/2}$. To eliminate ζ from the left-hand side of (2.15) we use the differential equation

$$\frac{d\chi}{d\zeta}=-CT\frac{(\chi^2-A^2)^{1/2}}{\chi+\frac{1}{2}}, \tag{2.22}$$

which follows from (2.11) and (2.18).

The price to be paid for the above change of variable manifests itself in the awkwardness of the boundary conditions. For $\chi=\frac{1}{2}x^2(1+R)-A^2$ we have $Q=R^{-1/2}$, while for the value of χ that is a solution of

$$[(\chi^2-A^2)^{1/2}+\chi]\exp[2(\chi^2-A^2)^{1/2}] =(x^2-A^2)\exp(2CT+Tx^2), \tag{2.23}$$

one must impose the constraint $Q=R^{1/2}$. After elimination of the spatial variable ζ the coefficients of the Riccati equation become rather lengthy. To be specific, the Riccati equation (2.15) then gets the form

$$\begin{aligned}\frac{dQ}{d\chi}=&-\frac{Q^2+1}{8A(\chi^2-A^2)^{1/2}(2\chi+A^2+1)^{1/2}}\left[(1+\lambda_\perp^{-1})\left[(2\chi+1)+\frac{4\chi^2-4A^2-1}{1-\lambda_p}\right.\right.\\&\left.\left.+\frac{(2\chi+1)(4\lambda_p^{-2}\chi^2-4\lambda_p^{-2}A^2-1)}{4(1-\lambda_p^{-1})W_\lambda}\right]+4\lambda_\perp^{-1}A^2\right]\\&+\frac{\lambda_\perp^{-1}Q+\hat{\lambda}(2\chi+1)Q}{(\chi^2-A^2)^{1/2}}-\frac{(1+\lambda_\perp^{-1})Q}{4A^2(\chi^2-A^2)^{1/2}(2\chi+A^2+1)}\\&\times\left[(2\chi+1)(\chi+A^2)-\frac{\chi+A^2+4(\chi^2-A^2)+4(\chi+A^2)(\chi^2-A^2)}{1-\lambda_p}\right.\\&\left.-\frac{(2\chi+1)[\chi+A^2+4\lambda_p^{-1}(\chi^2-A^2)+4\lambda_p^{-2}(\chi+A^2)(\chi^2-A^2)]}{4(1-\lambda_p^{-1})W_\lambda}\right],\end{aligned} \tag{2.24}$$

with the definition $\hat{\lambda}=\lambda L/(cCT)$. All results presented in the next section have been obtained by performing a numerical integration of this differential equation.

In the regime of vanishing ratios $c/(\gamma_\perp L), c/(\gamma_\parallel L)$ of the medium response times and the cavity round-trip time, usually referred to as the adiabatic case, the stability problem becomes a lot simpler. In this limit the Riccati equation (2.24) read

$$\frac{dQ}{d\chi}=-\frac{2A(2\chi+A^2+1)^{1/2}}{(2\chi+1)^2(\chi^2-A^2)^{1/2}}(Q^2+1)+\frac{\hat{\lambda}(2\chi+1)}{(\chi^2-A^2)^{1/2}}Q-\frac{4\chi^3-\chi(12A^2+3)-(4A^4+6A^2+1)}{(2\chi+A^2+1)(2\chi+1)^2(\chi^2-A^2)^{1/2}}Q\ , \tag{2.25}$$

with boundary conditions as mentioned above. This equation gets a simpler form if we transform Q according to

$$\tilde{Q}=\frac{A(2\chi+A^2+1)^{1/2}}{(\chi^2-A^2)^{1/2}-\chi-A^2}Q\ ,\qquad S=\frac{1}{(\chi^2-A^2)^{1/2}}\frac{\tilde{Q}-1}{\tilde{Q}+1}\ . \tag{2.26}$$

In this way we get rid of the square-roots and end up with the following differential equation

$$2(2\chi+1)^2(\chi^2-A^2)\frac{dS}{d\chi}=-S^2(\chi^2-A^2)[2+\hat{\lambda}(2\chi+1)^3]-2S(4\chi^3+8\chi^2+\chi-4A^2)+[8\chi+8A^2+2+\hat{\lambda}(2\chi+1)^3]\ . \tag{2.27}$$

A Riccati equation can completely be solved if a particular solution is available.[22] To investigate whether such a solution in terms of well-known functions exists for (2.27) we transform the latter in a standard way to a second-order linear differential equation. This equation turns out to possess seven singularities of which one is irregular and six are regular. The irregular singularity cannot be transformed away unless λ equals zero. It may thus be doubted whether the solution of (2.27) can be written in terms of well-known functions. This statement holds *a fortiori* for the nonadiabatic Riccati equation.

The special case $\lambda=0$ has already been investigated in Ref. 16. There we showed that for $\lambda=0$ the linearized Maxwell-Bloch equations can be solved with the help of the stationary solutions. Hence, it is not surprising that (2.27), with $\lambda=0$, has got a simple particular solution, which is given by $S=\chi^{-1}$. If we calculate the complete solution of the Riccati equation for this special case, we indeed find agreement with results obtained from stationary theory.

III. SIDE-MODE INSTABILITIES

In a previous article[16] we have demonstrated that the resonant mode is unstable in the negative-slope part of the bistability curve. In this section we shall locate instabilities which are generated by the side modes. In particular, we wish to determine whether a positive-slope portion of the stationary transmission curve can become unstable.

The conclusions in this section are based on numerical work, since it was observed above that for $\mathrm{Im}\lambda\neq 0$ analytical treatment of the stability problem is beyond our reach. The Riccati equation (2.24) has been integrated with the help of a Merson routine[23] and the result has been matched to the condition mentioned below (2.23) by means of a root-finding program. We largely confined ourselves to the first side mode and to the case $d=1$, with d standing for the ratio $\gamma_\parallel/\gamma_\perp$. Furthermore, we chose values of the cooperation parameter that are less than 500.

The transmission coefficient T of the mirrors is a parameter of major importance for the occurrence of side-mode instabilities in a Fabry-Pérot cavity. The first proof of this statement is provided by Fig. 1. It shows the nearest-side-mode instability regions in the $(x,\tau_\perp)$ plane for a bistable system with $C=140$, $d=1$ and mirror transmittivity $T=0$ and $T=0.05$, respectively. The quantity x is the output amplitude, while $\tau_\perp$ denotes the ratio $c/(L\gamma_\perp)$. The large island in Fig. 1 is the instability domain for $T=0$. Its boundary curve has been computed from the uniform-field theory, discussed in Ref. 16. For $T=0.05$ two disconnected domains are present, one inside the uniform-field domain, which we shall name accordingly, and another in the neighborhood of the x axis. Since $\tau_\perp=0$ corresponds to the adiabatic limit, we shall refer to the latter instability region as the "adiabatic" domain from now on. It thus appears that for increasing transmission coefficient the uniform-field instability domain shrinks, whereas a new instability domain starts growing elsewhere in the $(x,\tau_\perp)$ plane. As a consequence the system may become unstable even in the adiabatic limit. Such adiabatic instabilities do not exist in the uniform-field approximation, as has been proven analytically.[11] It should be noted that the simultaneous presence of several disconnected instability domains as found here is not a new feature; it has also been reported for

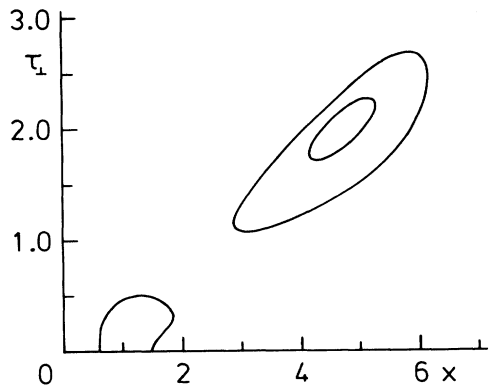

FIG. 1. Instability domains for the first side mode at $C=140$ and $d=1$. The large island corresponds to $T=0$, the small island and the domain at the x axis to $T=0.05$.

dispersive optical bistability in a ring cavity.[24]

As a check on our numerical results we have also determined the nearest-side-mode instability domain in the $(x,\tau_\perp)$-plane for $T=0.01$, and for the same values of C and d as in Fig. 1. In this case the adiabatic region is not yet present; the curve bounding the uniform-field region lies close to the curve for $T=0$, as expected. Additional numerical insight in the convergence of the results for small T is acquired by calculating the minimum x value of the uniform-field domain. At $T=0.05$ this value differs by 50% from that found for $T=0$; at $T=0.01$ the deviation is only 5.3%.

The difference between the predictions of uniform-field theory and our numerical results at $T=0.05$ is visualized in Fig. 2, where the real and imaginary parts of the eigenvalue $\lambda L/c$ are plotted as a function of x for fixed values of $\tau_\perp$, C, and $d=1$. For $T=0$ the real part of $\lambda L/c$ increases monotonously and never exceeds zero. However, for $T=0.05$ a positive-valued maximum is attained, in accordance with the presence of the adiabatic domain in Fig. 1. The behavior of $\mathrm{Im}(\lambda L/c)$ at $T=0.05$ is also quite different from the uniform-field prediction, which is $\mathrm{Im}(\lambda L/c)=\pi$. For x equal to zero $\lambda L/c$ is determined

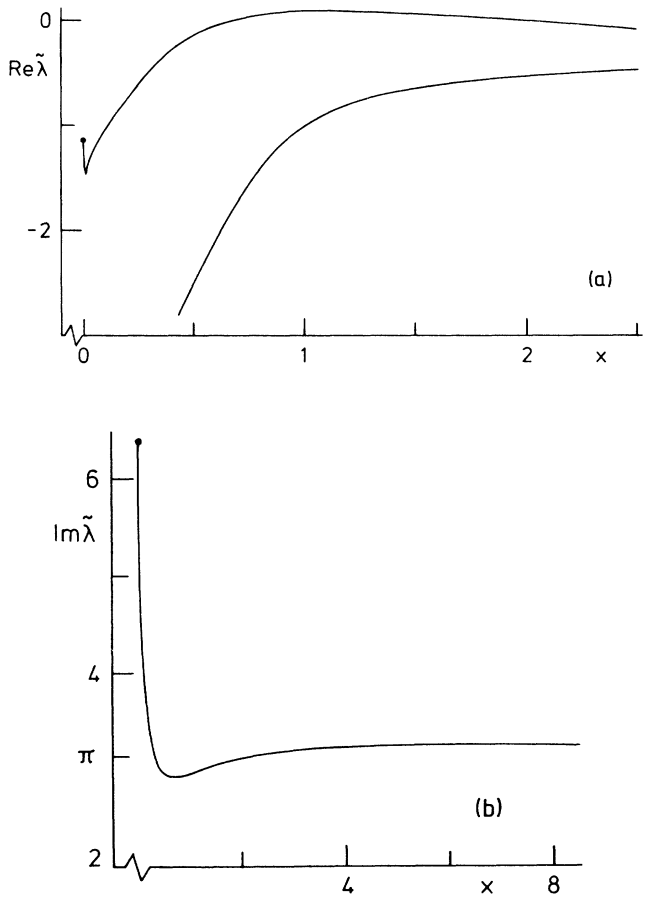

FIG. 2. Real and imaginary parts of the eigenvalue $\lambda L/c$ as a function of x, for $T=0.05$, $\tau_\perp=0.3$, $C=140$, and $d=1$. The lower curve in the plot of $\mathrm{Re}(\lambda L/c)$ is the uniform-field result that is valid for $T=0$.

TABLE I. Threshold values of the cooperation parameter C at which nearest-side-mode instabilities appear for $d=1$.

T	Uniform-field domain	Adiabatic domain
0	96.9	∞
0.05	132	112
0.1	274	57.7
0.2	>500	31.0

by the formula

$$\frac{\lambda L}{c}=\frac{\sigma\tau_\perp-1+[(\sigma\tau_\perp+1)^2-4CT\tau_\perp]^{1/2}}{2\tau_\perp}, \tag{3.1}$$

with $\sigma=\frac{1}{2}\ln R+\pi n i$ and n an integer. If we take $n=1$, $T=0.05$, $\tau_\perp=0.3$, and $C=140$, we find $\lambda L/c=-1.14+6.40i$. This is in agreement with the numerical results for $\lambda L/c$ at small x. The fact that 6.40 is much higher than π can be explained by taking into consideration that for $n=0$ Eq. (3.1) yields $\mathrm{Im}(\lambda L/c)=4.54$; thus as x approaches zero the imaginary part of the first-side-mode eigenvalue is pushed upwards by the resonant mode.

The findings shown in Fig. 1 give rise to the question for which values of the cooperation parameter C the adiabatic and the uniform-field instability domains come into being. The answer is given by Table I. The threshold values for C critically depend on the choice of the transmission coefficient T. If this quantity increases, the threshold for the appearance of the uniform-field region rises rapidly towards experimentally inaccessible high values, whereas the threshold for the presence of the adiabatic region drops down to rather low values.

Table I has been computed for the case that the ratio d of the medium damping coefficients equals unity. In the uniform-field approximation we have found[16] that the choice of d influences the instability spectrum, albeit rather weakly. In Table II evidence is given to the fact that the same is true for a finite transmission coefficient. The threshold values of C for the appearance of the adiabatic domain decrease by some 20% if d grows from 0.5 towards 2.

If d is varied, not only the threshold values for C change but the points in the $(x,\tau_\perp)$ plane where instabilities start developing move as well. For $d=0.5$ the adiabatic domain contracts towards a point on the x axis as C approaches its threshold value. For higher values of d the adiabatic domain shrinks towards a point above the x axis. The pictures in Fig. 3 confirm these statements for $T=0.1$; at other values of T the behavior of the adiabatic

TABLE II. Threshold values of the cooperation parameter C at which the adiabatic domain for the nearest side mode appears.

T	$d=0.5$	$d=2$
0.05	115	90.3
0.1	59.6	47.0
0.2	32.4	25.6

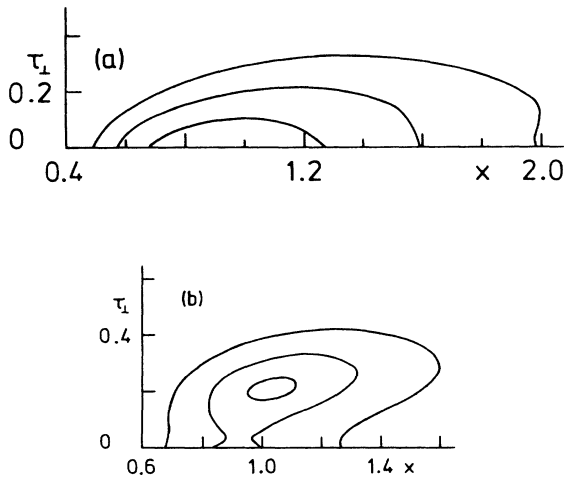

FIG. 3. Adiabatic instability domains for $T=0.1$. The first picture shows the cases $d=0.5$, $C=65$, 75, 90 and the second $d=1$, $C=58$, 60, 65. The outer curves correspond to the highest C value.

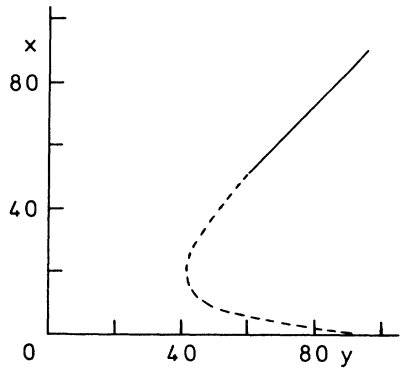

FIG. 5. Stationary transmission curve for $T=0.1$ and $C=450$. The dashed part is unstable.

domain is qualitatively the same. In studying Fig. 3 one must bear in mind that for $\tau_\perp=0$ the stability problem does not depend anymore on d.

As it is clear by now where the nearest-side-mode instability domains are located in the $(x,\tau_\perp)$ plane for various T, C, and d, we turn our attention to the issue of positive-slope instabilities. These are instabilities in the cooperative or the one-atom branch of the stationary transmission curve, which are experimentally accessible. For the Fabry-Pérot cavity positive-slope instabilities have solely been predicted on the basis of simplified semiclassical models.[2,4,8,9] The full Maxwell-Bloch theory predicts that positive-slope instabilities are not present in an optically bistable system that is enclosed in a Fabry-Pérot cavity with ideal mirrors.[12,16] We can now check whether this prediction of Maxwell-Bloch theory still holds if the transmission coefficient T takes finite values.

In the adiabatic limit, which corresponds to $\tau_\perp=0$, one may argue that positive-slope instabilities will be absent for a cavity with nonideal mirrors as well. In fact, if we set $\mathrm{Re}\lambda$ equal to zero in (2.27), let C tend to infinity and assume that $\mathrm{Im}\lambda$ remains finite as C approaches infinity, the stability problem becomes the same for the resonant mode and all side modes. This suggests that for finite C the side modes cannot generate positive-slope instabilities, a conclusion which is indeed supported by our numerical results.

In order to determine whether positive-slope instabilities are present for finite T in the nonadiabatic case we have followed the adiabatic and the uniform-field domains of Fig. 1 in parameter space and computed these domains for various $C<500$, with $T=0.1$ and $d=1$. The result at $C=450$ is shown in Fig. 4. The island is the uniform-field domain. It is located well inside the strip containing the points with x values that correspond to the negative-slope part of the bistability curve. Hence, the uniform-field domain does not give rise to positive-slope instabilities. This fact is not surprising, since we have seen above that such instabilities are absent for $T=0$ and that the uniform-field domain shrinks with increasing values of T. In contrast, the adiabatic domain in Fig. 4 extends from $x=0.0649$ towards $x=50.9$, while the positive-slope branches of the bistability curve are bounded by $x=0.254$ and $x=19.5$ for $T=0.1$ and $C=450$. Hence, this domain causes instabilities in both the cooperative and the one-atom branch. In Fig. 5 the unstable part of the steady-state curve has been indicated for the chosen values of T and C; the figure shows that a

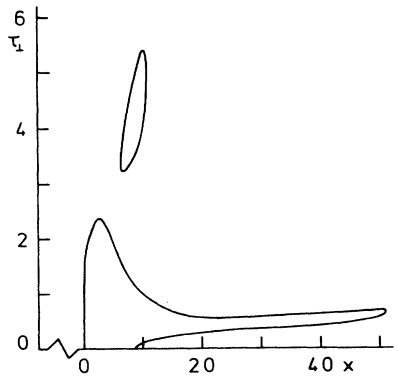

FIG. 4. Nearest-side-mode instability regions for $T=0.1$, $C=450$, and $d=1$.

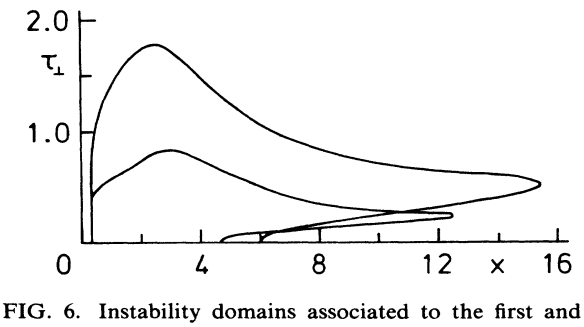

FIG. 6. Instability domains associated to the first and the second side mode, for $T=0.2$, $C=150$, and $d=1$. The larger domain refers to the first side mode.

TABLE III. Response times and frequency gaps for $d=1$.

	$T=0.1$, $C=450$			$T=0.2$, $C=150$		
x	10	30	50	7	11	15
$t_R(\times 10^2 L/c)$	0.072	1.4	20	0.082	0.31	4.6
$\Delta\omega(\times c\pi/L)$	0.990	0.993	0.993	0.987	0.990	0.990

substantial portion of the upper transmission branch is unstable.

If we increase the transmission coefficient to 0.2, we encounter positive-slope instabilities already at $C=150$ for $d=1$. In Fig. 6 both the instability domains associated to the first and the second side mode have been drawn. For the time being we concentrate on the first-side-mode instability domain. At the chosen values of C and d the uniform-field domain does not exist (see Table I). First-side-mode instabilities occur for $x\in[0.301, 15.5]$, while the negative-slope part of the stationary transmission curve is given by $x\in[0.305, 10.3]$. The consequences for the bistability curve are shown in Fig. 7; again the one-atom branch is unstable for a considerable part.

To get an idea of the time scales and the frequencies connected with the upper-branch instabilities of Figs. 4 and 6, we have computed the scaled eigenvalue $\lambda L/c$ as a function of $\tau_\perp$, for a few values of x. The maximum value of $\mathrm{Re}(\lambda L/c)$ and the associate imaginary part of $\lambda L/c$ have been used to calculate the response time t_R for the instabilities and the frequency gap $\Delta\omega$ between the resonant mode and the first side mode. From Table III we infer that a typical response time for upper-branch instabilities amounts to 100 cavity round-trip times. Inside the negative-slope region the response time is on average shorter by a factor 10. The frequency gaps $\Delta\omega$ are close to the free spectral range throughout.

To assess the importance of the positive-slope instabilities we need information on the values for C at which these instabilities show up. From Table IV it is observed that the threshold for positive-slope instabilities lowers sharply if the transmission coefficient increases. This effect is almost completely due to the dynamics and not to the statics of the Maxwell-Bloch equations: for instance, if we set C equal to 113 and increase T from 0.1 to 0.2 the maximum x value of the adiabatic domain vastly increases, from 3.36 to 8.89, whereas the x coordinate of the upper turning point of the bistability curve decreases merely from 9.67 to 8.89. In connection with Table IV it is interesting to remark that for the case of a ring cavity with $T=0.1$ and $d=1$ positive-slope instabilities occur already at C values that are an order of magnitude smaller.[25]

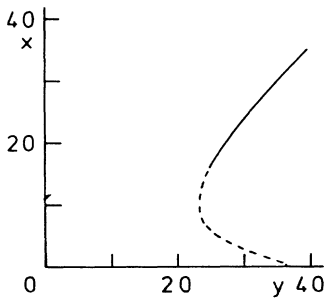

FIG. 7. Stationary transmission curve for $T=0.2$ and $C=150$. The dashed part is unstable.

The stability of the nearest side mode has now been investigated in some detail. Generally, one expects this mode to generate the largest instability domain as compared to the higher side modes. The reason for this presumption lies in the fact that if $|\mathrm{Im}(\lambda L/c)|\to\infty$ we have $\mathrm{Re}(\lambda L/c)=\frac{1}{2}\ln R$, so that side-mode instabilities die out as $\mathrm{Im}(\lambda L/c)$ becomes large. To obtain some numerical information on the behavior of the higher-side modes we have drawn, in Fig. 6, besides the nearest side-mode instability region the instability domain for the second side mode as well. Clearly, this domain is smaller than that belonging to the first side mode. Instabilities are present for $x\in[0.306, 12.5]$, so that at $T=0.2$, $C=150$, and $d=1$ both the first and the second side mode can cause instabilities in the upper branch of the bistability curve.

Recently[13-15] experiments have been carried out which enable one to verify predictions of the Maxwell-Bloch theory on side-mode instabilities in optical bistability. For a dispersive medium in a Fabry-Pérot cavity self-pulsing behavior has been observed in the upper branch of the bistability curve, whereas for the purely absorptive case no instabilities have been found.[15] The latter experimental fact can be used to test the present theory on instabilities in a Fabry-Pérot cavity. To that end we have computed $\mathrm{Re}(\lambda L/c)$ as a function of x for experimental values of the physical parameters, viz., $T=0.31$, $C=294$, $\tau_\perp=11.5$, and $d=1$. For $x\leq 50$ the real part of the eigenvalue λ never exceeds -0.1, so that under the above mentioned conditions nearest-side-mode instabilities do not exist. Hence, the negative outcome of the experimental search for instabilities in purely absorptive optical bistability is in accordance with the present theory. For completeness, we have calculated the boundaries of the

TABLE IV. Threshold values for C at which positive-slope instabilities for $d=1$ emerge.

T	Lower branch	Upper branch
0	∞	∞
0.05	483	>500
0.1	246	399
0.2	128	113

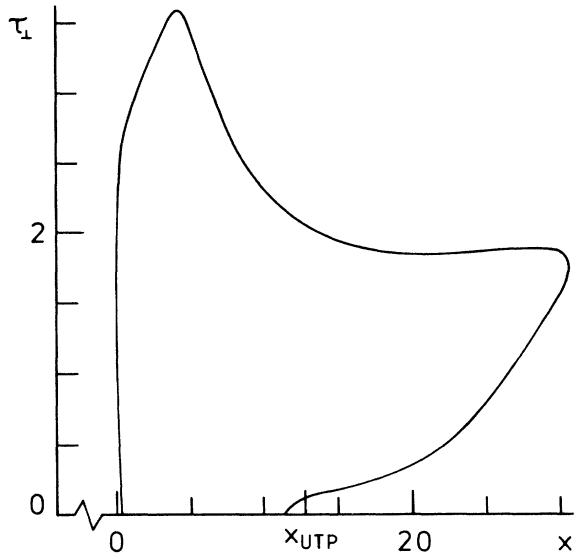

FIG. 8. Nearest-side-mode instability domain for $T=0.31$, $C=294$, and $d=1$. The x coordinate of the upper turning point of the bistability curve, denoted by the symbol x_{UTP}, is slightly higher than the upper boundary of the instability domain for $\tau_\perp=0$.

nearest-side-mode instability domain in the $(x,\tau_\perp)$ plane, at the same values for T, C, and d. The result is shown in Fig. 8. Upper-branch instabilities are only present for $\tau_\perp$ of the order of unity, which is far from the experimental values.

The absence of nearest side-mode instabilities in the absorptive case for dimensionless medium response-times $\tau_\perp$ of the order of 10 and at the chosen values of T, C, and d is a characteristic feature of the standing-wave geometry used in the experiment. To demonstrate this we have calculated the instability domain for the case of a folded unidirectional cavity of length $2L$, which is sometimes used to model a Fabry-Pérot cavity of length L.[15] For such a configuration the eigenvalue λ follows from[16,26,27]

$$\frac{\lambda L}{c}=\pi n i+\tfrac{1}{2}\ln R+\tfrac{1}{4}(1+\lambda_\perp^{-1})\ln\left[\frac{\lambda_p+x^2\eta^2}{\lambda_p+x^2}\right]-\tfrac{1}{2}\lambda_\perp^{-1}\ln\eta\ , \tag{3.2}$$

where n is an integer and η must be calculated from

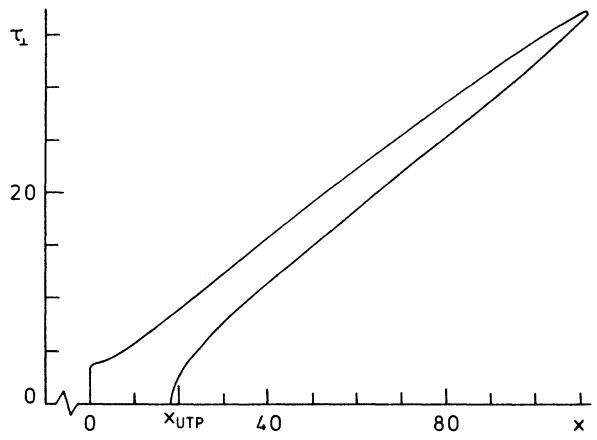

FIG. 9. Nearest-side-mode instability domain at $T=0.31$, $C=587$, and $d=1$ for the case of a folded unidirectional cavity of length $2L$. The x coordinate of the upper turning point of the bistability curve coincides with the upper boundary of the instability domain for $\tau_\perp=0$.

$$\ln\eta+\tfrac{1}{2}x^2(\eta^2-1)=CT\ . \tag{3.3}$$

In Fig. 9 the instability domain is displayed as it is determined by the above equations with $T=0.31$, $C=587$, $d=1$, and $n=1$. Incidentally, it should be borne in mind that we have adopted the definition $C=\alpha L/T$, with α the medium absorption coefficient, both for a ring and a Fabry-Pérot cavity of length L. In comparing Figs. 8 and 9 one should notice the different scales for x and $\tau_\perp$. It turns out that in a folded ring configuration, in which standing-wave effects are not present, upper-branch instabilities exist for values of $\tau_\perp$ up to 37. In contrast, upper-branch instabilities already disappear for $\tau_\perp$ greater than 2.0 in a standing-wave cavity.

In conclusion, we have shown that Maxwell-Bloch theory can furnish an adequate description of instabilities of an optically bistable system in a nonideal Fabry-Pérot cavity provided that both spatial inhomogeneities and standing-wave effects are fully taken into account. If, in contrast, one resorts to uniform-field theory, the existence of an "adiabatic" instability domain is ignored and a complete absence of positive-slope instabilities is predicted. If one neglects the fields propagating backwards the adiabatic domain blows up, so that the extent of positive-slope instabilities is overestimated.

[1]For a review, see, e.g., L. A. Lugiato, in *Progress in Optics XXI*, edited by E. Wolf (North-Holland, Amsterdam, 1984), p. 69; H. M. Gibbs, *Optical Bistability: Controlling Light with Light* (Academic, Orlando, 1985); L. A. Lugiato, C. Oldano, L. M. Narducci, and R. Lefever, in *Instabilities and Chaos in Quantum Optics II*, edited by N. B. Abraham, F. T. Arecchi, and L. A. Lugiato (Plenum, New York, 1988), p. 231.

[2]W. J. Firth, Opt. Commun. **39**, 343 (1981).

[3]E. Abraham, W. J. Firth, and J. Carr, Phys. Lett. **91A**, 47 (1982).

[4]E. Abraham and W. J. Firth, Opt. Acta **30**, 1541 (1983).

[5]K. Ikeda and M. Mizuno, Phys. Rev. Lett. **53**, 1340 (1984).

[6]K. Ikeda and M. Mizuno, IEEE J. Quantum Electron. **21**, 1429 (1985).

[7]J. A. Goldstone and E. M. Garmire, IEEE J. Quantum Electron. **17**, 366 (1981).

[8]J. A. Goldstone and E. M. Garmire, IEEE J. Quantum Electron. **19**, 208 (1983).
[9]F. Casagrande, L. A. Lugiato, and M. L. Asquini, Opt. Commun. **32**, 492 (1980).
[10]M. Sargent III, Kvant. Elektron. (Moscow) **7**, 2151 (1980) [Sov. J. Quantum Electron. **10**, 1247 (1980)].
[11]H. J. Carmichael, Opt. Commun. **53**, 122 (1985).
[12]S. Maize, B. V. Thompson, and S. S. Hassan, in *Optical Bistability III,* edited by H. M. Gibbs, P. Mandel, N. Peyghambarian, and S. D. Smith (Springer, Berlin, 1986), p. 352.
[13]B. Ségard and B. Macke, in *Optical Bistability IV,* edited by W. Firth, N. Peyghambarian, and A. Tallet (Editions de Physique, Les Ulis, 1988), p. 371.
[14]B. Ségard and B. Macke, Phys. Rev. Lett. **60**, 412 (1988).
[15]B. Ségard *et al.*, Phys. Rev. A **39**, 703 (1989).
[16]A. J. van Wonderen, B. J. Douwes, and L. G. Suttorp, Physica (Utrecht) **A157**, 907 (1989).
[17]L. A. Lugiato and L. M. Narducci, Z. Phys. B **71**, 129 (1988).
[18]For a recent paper on the influence of transverse effects in a ring cavity, see L. A. Orozco *et al.*, Phys. Rev. A **39**, 1235 (1989).
[19]L. G. Suttorp and A. J. van Wonderen, in Technical Digest of the First European Quantum Electronics Conference, Hannover, FRG, 1988 (unpublished).
[20]W. Magnus, F. Oberhettinger, and R. P. Soni, *Formulas and Theorems for the Special Functions of Mathematical Physics* (Springer, Berlin, 1966).
[21]J. A. Hermann, Opt. Acta **27**, 159 (1980).
[22]E. L. Ince, *Ordinary Differential Equations* (Dover, New York, 1926).
[23]*Modern Numerical Methods for Ordinary Differential Equations,* edited by G. Hall and J. M. Watt (Clarendon, Oxford, 1976).
[24]M. L. Asquini, L. A. Lugiato, H. J. Carmichael, and L. M. Narducci, Phys. Rev. A **33**, 360 (1986).
[25]M. Gronchi *et al.*, Phys. Rev. A **24**, 1419 (1981).
[26]H. J. Carmichael, Phys. Rev. A **28**, 480 (1983).
[27]L. A. Lugiato *et al.*, Phys. Rev. A **32**, 1563 (1985).